


Thermal transport across nanoscale damage profile in sapphire irradiated by swift heavy ions

Cite as: J. Appl. Phys. **127**, 035108 (2020); <https://doi.org/10.1063/1.5126413>

Submitted: 02 September 2019 . Accepted: 13 December 2019 . Published Online: 21 January 2020

 A. Abdullaev,  V. S. Chauhan,  B. Muminov,  J. O'Connell,  V. A. Skuratov,  M. Khafizov, and  Z. N. Utegulov

COLLECTIONS

 This paper was selected as Featured

 This paper was selected as Scilight



View Online



Export Citation



CrossMark

ARTICLES YOU MAY BE INTERESTED IN

[Studying thermal conductivity after irradiation](#)

Scilight **2020**, 041102 (2020); <https://doi.org/10.1063/10.0000628>

[Spatially resolved thermoreflectance techniques for thermal conductivity measurements from the nanoscale to the mesoscale](#)

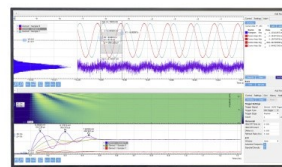
Journal of Applied Physics **126**, 150901 (2019); <https://doi.org/10.1063/1.5120310>

[Phonon properties and thermal conductivity from first principles, lattice dynamics, and the Boltzmann transport equation](#)

Journal of Applied Physics **125**, 011101 (2019); <https://doi.org/10.1063/1.5064602>

Challenge us.

What are your needs for
periodic signal detection?



Zurich
Instruments

Thermal transport across nanoscale damage profile in sapphire irradiated by swift heavy ions



Cite as: J. Appl. Phys. 127, 035108 (2020); doi: 10.1063/1.5126413

Submitted: 2 September 2019 · Accepted: 13 December 2019 ·

Published Online: 21 January 2020



A. Abdullaev,¹ V. S. Chauhan,² B. Muminov,³ J. O'Connell,⁴ V. A. Skuratov,^{5,6,7} M. Khafizov,^{2,a)} and Z. N. Utegulov^{1,b)}

AFFILIATIONS

¹Department of Physics, School of Sciences and Humanities, Nazarbayev University, Nur-Sultan 010000, Kazakhstan

²Department of Mechanical and Aerospace Engineering, Ohio State University, Columbus, Ohio 43210, USA

³Department of Mechanical Engineering, University of California, Riverside, California 92521, USA

⁴Centre for HRTEM, Nelson Mandela University, Port Elizabeth 6001, South Africa

⁵Flerov Laboratory of Nuclear Reactions, Joint Institute for Nuclear Research, Dubna, Moscow Region 141980, Russia

⁶Division of Nuclear Physics and Technologies, National Research Nuclear University MEPhI, Moscow 115409, Russia

⁷Faculty of Natural and Engineering Science, Dubna State University, Dubna, Moscow Region 141980, Russia

^{a)}E-mail: khafizov.1@osu.edu

^{b)}E-mail: zhutegulov@nu.edu.kz

ABSTRACT

We studied the degradation of thermal conductivity in single crystal sapphire ($\alpha\text{-Al}_2\text{O}_3$) irradiated by 167 MeV Xe *swift heavy ions* (SHIs) over the multiple fluences in the range of 10^{12} – 10^{14} ions/cm². Thermal conductivity was measured primarily in the cross-plane direction using a noncontact ultrafast optical pump-probe technique called picosecond time domain thermoreflectance (TDTR). Multiple samples with variable ion fluences allowed us to probe distinct regions resulting from different regimes of microstructure evolution caused by *electronic energy loss*. By tuning the penetration depth of the thermal waves using different modulation frequencies, two regions with distinct conductivities were identified and the values of which were found to be consistent with phonon-mediated thermal transport models while the microstructure was confirmed by electron microscopy characterization. These damaged regions were determined to be a several micrometer thick *ion track region* and several tens of nanometer-thick *amorphous layer* present only above 5.0×10^{13} ions/cm². These results demonstrate the applicability of TDTR to resolve thermal transport behavior in SHI irradiated oxides having nonhomogeneous damage profile on a nanometer scale. The presented approach facilitates future studies aiming at resolving the impact of distinct damage resulting from electronic and nuclear stopping regimes under irradiation.

Published under license by AIP Publishing. <https://doi.org/10.1063/1.5126413>

I. INTRODUCTION

Methods utilizing energetic ions, such as ion implantation to introduce dopants and ion beam lithography to pattern nanostructures, have been extensively used for electronic and optoelectronic applications.^{1–4} Additionally, the potential of high energy ions induced microstructure to tailor material properties for a wide range of applications has been investigated.^{5–7} Propagation of energetic ions in insulators is divided into two regimes: electronic and nuclear stopping, where ions are slowed down by transfer of energy to either electrons or the nuclei of target materials' atoms, respectively. Impact

of these regimes on defect production and microstructure evolution is extensively discussed.

From the thermal management perspective, the ability to control thermal conductivity of material has attracted a lot of attention. This control is especially useful in the areas of thermoelectrics, electronics, and ceramics for advanced energy systems.^{8–10} Recently, the importance of single-effect studies for development of predictive thermal transport models in ceramics under irradiation has been recognized.^{11–13} These studies have been enabled by the development of new experimental approaches that can be used on ion beam

irradiated samples with tailored microstructure to measure physical properties of the damaged layer.^{14–16} These early studies primarily focused on a damage resulting from displacement damage caused by the elastic nuclear stopping process induced by a few million electron volt energy ions. Currently, very little is known about the impact of damage resulting from inelastic electronic stopping on thermal conductivity.^{5,17} Under irradiation with swift heavy ions (SHIs), electronic and nuclear stopping regimes are spatially isolated, which makes them well-suited for addressing the above need. Additionally, bombardment with high energy ions offers a unique opportunity to simulate fission fragment-induced damage and its impact on thermal transport.^{18,19}

Energetic ions bombarded into ceramic materials are initially slowed by electronic interaction where the ion excites electrons of the insulating material.^{20,21} These excited electrons thermalize by transferring their energy to the lattice, which results in local heating around the ion trajectory. Above a certain energy threshold, the amount of deposited energy is too large to be dissipated and the material undergoes localized melting resulting in latent track formation.^{22–24} The ability of SHIs to produce aligned ion tracks can also be utilized as a tool to tailor physical properties of insulating ceramics, which can be useful for electronics applications.

In addition to practical importance, experimental data on the SHI induced changes in thermal properties are of interest for development and validation of models describing damage evolution mechanism along ion track trajectory. In particular, it has been demonstrated in many reports that the electronic energy loss threshold for latent track formation scales with the value of thermal conductivity of the corresponding pristine material.²⁵

Traditionally, thermal property assessment of irradiated materials has been achieved using a laser flash technique, which provides resolution on a millimeter scale and is suitable for neutron irradiated samples with a uniform damage profile.²⁶ For micrometer scale resolution, modulated thermoreflectance microscopy utilizing continuous wave lasers with pump modulation frequencies ranging from 10 kHz to 1 MHz has been shown to provide the necessary resolution to resolve thermal transport in ion irradiated samples whose damage is confined to a few micrometers on the irradiated surface.^{15,17,27} To explore thermal transport degradation in irradiated structures with nanometer scale damage profiles, techniques utilizing pulsed lasers such as picosecond time domain thermoreflectance (TDTR) with modulation rates in excess of 1 MHz^{28–30} and transient grating,^{14,16} as well as the electron beam heating technique,³¹ have been employed.

In this work, we explore the utilization of SHI induced ion tracks to tailor thermal transport properties of insulators. To the best of our knowledge, this is the first report where thermal conductivity of different radiation damaged zones resulting from electronic stopping is depth-resolved on a nanometer scale using the TDTR approach. Also, we have not found any previous reports of thermal conductivity degradation due to ion tracks associated with SHI radiation damage. Here, we study the degradation of cross-plane thermal conductivity in sapphire (α - Al_2O_3) irradiated by SHIs using frequency-dependent TDTR and characterize the microstructure of subsurface layers using the thermal transport model. We demonstrate the importance of TDTR for the analysis of an insulator with ion tracks, especially at higher doses, where a few nanometer-thick amorphous subsurface layer proliferates.

II. EXPERIMENT

A. Sample structure

High purity polished single crystal c-cut (0001) sapphire samples of 0.5 mm thickness and ($10 \times 5 \text{ mm}^2$) area were purchased from the MTI Corporation. The samples were irradiated at 60 °C with 167 MeV Xe ions along the c-axis with fluences in the range of 10^{12} – 10^{14} ions/cm² using the IC-100 FLNR JINR cyclotron facility in Dubna, Russia. This energy corresponds to the initial electronic stopping power $\sim 24 \text{ keV/nm}$. Ion beam homogeneity better than 5% on irradiating specimen surface has been reached using beam scanning in horizontal and vertical directions. An average Xe ion flux of $2.3 \times 10^9 \text{ cm}^{-2} \text{ s}^{-1}$ was continuously monitored by measuring the ion beam current using a Faraday cup to an accuracy of 15%. The samples were mounted on water-cooled copper holders, maintained at 25–30 °C, using a double sided carbon tape. The temperature rise in Al_2O_3 due to Xe irradiation was determined in reference experiments using thermocouples attached to the samples.

Figure 1 presents cross-sectional (a) and plane-view (b) bright field TEM images of swift Xe ion-induced latent tracks in sapphire at 2.0×10^{12} and 2.0×10^{10} ions/cm², respectively. In accordance with previous observations,²² the tracks are discontinuous, highly porous regions along ion trajectories [Fig. 1(a)], likely formed during solidification of the molten material. Figure 1(b) was taken at low (2.0×10^{10} ions/cm²) ion fluence, to isolate individual tracks and demonstrate crystalline nature of single latent track.

B. Experimental setup

To perform near surface nanoscale thermal transport measurement on irradiated sapphire samples, we have implemented the TDTR setup.²⁵ The Ti:Al₂O₃ mode-locked femtosecond laser (Tsunami, Spectra Physics) at 782 nm wavelength, 80 MHz repetition rate and 80 fs pulse duration, was used as pump and probe beams. Modulation frequency-dependent TDTR^{32,33} was performed by tuning the pump modulation frequency within a 1–10 MHz frequency range, with corresponding RLC filter [an electrical circuit consisting of a resistor (R), an inductor (L), and a capacitor (C)]

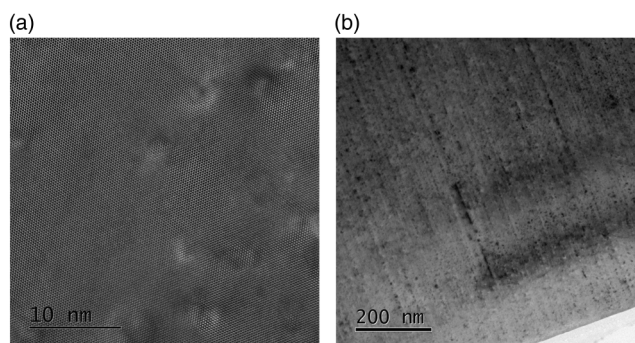


FIG. 1. TEM images of latent tracks in sapphire irradiated by 167 MeV Xe ions. (a) Bright field (BF) cross-sectional TEM (XTEM) image of tracks at a fluence of $2.0 \times 10^{12} \text{ cm}^{-2}$. (b) High resolution plain-view image of tracks at a fluence of $2.0 \times 10^{10} \text{ cm}^{-2}$.

for each modulation frequency and phase adjustment of the lock-in amplifier.³⁴ Prior to these measurements, the RF magnetron sputtering was employed to sputter an 85 nm thick aluminum (Al) transducer layer, whose thickness was measured using picosecond acoustics. The surface roughness of SHI irradiated samples was negligibly low. Previous studies demonstrated the formation of small hillock defects of ~5 nm height on the top surface of sapphire irradiated by SHIs,^{35,36} thus with no affect to our measurements.

Recorded picosecond TDTR signal of $-V_{in}/V_{out}$ as a function of delay time between pump and probe beams was fitted with a thermal diffusion model to extract unknown thermal conductivity.³⁷ The thermal analysis was based on the iterative algorithm applied to a multilayer geometry with thermal conductivity, volumetric specific heat capacity, and thickness defined for each layer. The pump and probe beams had Gaussian radial profiles with $1/e^2$ diameters of 12.8 and 12.2 μm , respectively. The root mean square, $1/e^2$ beam diameter is measured to be ~12.4 μm . For modulation frequencies (1–10 MHz), the heat penetration depths were typically on the order of *hundreds of nanometers*, which are much smaller than the thickness of the subsurface ion irradiated region (approximately several micrometers), which enables us to probe thermal transport in the *near-surface* damaged region resulting from the electronic stopping regime. The aligned nature of ion track implies anisotropic thermal transport within that region. However, since cross-plane heat penetration depth is on the order of 1 μm and much smaller than the laser pump beam diameter, the subsurface temperature gradient is essentially one-dimensional, and measurement is primarily sensitive to cross-plane conductivity. While simultaneous measurement of in-plane and cross-plane conductivities using TDTR has been demonstrated in highly anisotropic materials, here an alternative approach is needed and is a subject of separate work.³⁸

III. MODELING

A. Phonon-mediated thermal transport model for pristine and SHI irradiated Al_2O_3

Thermal conductivity in dielectric solids such as sapphire is primarily governed by phonons and limited by intrinsic anharmonic processes and phonon scattering with defects.³⁹ To model cross-plane thermal conductivity k of pristine and irradiated Al_2O_3 , we used the semianalytical phonon-mediated kinetic theory model,^{39,40}

$$k = \frac{1}{3} \sum_{i=1}^3 \int_0^{\omega_{m,i}} \tau_{c,i}(\omega) v_i^2 C(T, \omega) D_i(\omega) d\omega, \quad (1)$$

where v_i is the phonon group velocity of each acoustic phonon branch (one longitudinal $v_1 = 8800$ m/s and two degenerate transverse $v_2 = 3988$ m/s⁴¹) $C(T, \omega)$ is the frequency-dependent specific heat of the phonon mode given by $C(T, \omega) = \frac{\hbar^2 \omega^2 e^{\hbar\omega/k_B T}}{k_B T^2 (e^{\hbar\omega/k_B T} - 1)^2}$, where \hbar is the reduced Planck constant, k_B is the Boltzmann constant, $D_i(\omega) = \frac{1}{2\pi^2} \frac{\omega^2}{v_i^3}$ is the phonon density of states, and $\tau_{c,i}(\omega)$ is the total phonon relaxation time.¹³ Equation (1) is derived using Debye's phonon density-of-states with assumption of a linear phonon dispersion curve having one longitudinal and two transverse acoustic branches. Maximum frequency of the phonons for each branch is

calculated as 9.5 and 5.6 THz, respectively, using the Debye expression $\omega_{m,i} = v_i(6\pi^2/\Omega_0)^{1/3}$, where $\Omega_0 = 8.51 \times 10^{-30} \text{ m}^{-3}$ is the atomic density. For simplification of analysis, we neglected the slight thermal anisotropy of pristine sapphire due to its trigonal crystal structure.⁴² Total phonon relaxation time is the combination of three-phonon, phonon-point defect, and phonon-boundary scattering processes added using the Mathieson's rule, $\tau_c^{-1} = \tau_{3ph}^{-1} + \tau_d^{-1} + \tau_B^{-1}$. Three-phonon or umklapp scattering process defines the phonon relaxation time, $\tau_{3ph}^{-1}(\omega) = B_i \omega^2 T$, which is the thermal resistance only due to crystal anharmonicity, where $B_i = \frac{2\gamma^2 k_B}{\Omega_0 \omega_{m,i}} \times \frac{1}{C_i}$ is the parameter associated with umklapp scattering and C_i is the elastic constant in i th direction. For the model, the value of elastic constants was taken from the literature as $C_{11} = 496$ GPa and $C_{44} = 148$ GPa.⁴³ The phonon scattering rate by intrinsic impurities is $\tau_d^{-1}(\omega) = A_0 \omega^4$, where A_0 is the measure of the strength of the phonon defect scattering. Lastly, the boundary term, τ_B^{-1} is due to phonon scattering with the boundaries of the *discontinuous latent tracks* generated by SHIs (Fig. 1). While a literature search did not reveal any expression particular to ion tracks, extensive literature exists considering thermal transport in low dimensional systems such as thin films and nanowires.^{9,44,45} We assume that the high density of well oriented tracks resembling a two-dimensional nanowire "forest" confines propagation of phonons in a similar manner as the boundaries of the nanowire and thin films, which leads to the following expression for the phonon-boundary scattering rate:⁴⁵

$$\tau_B^{-1} = \gamma_i \omega \frac{v_i}{D_a}. \quad (2)$$

This term captures phonon scattering characterized by a frequency-dependent specular reflection parameter with latent ion tracks,⁴⁴ where $\gamma_i = (\delta\beta\omega_{m,i})^{-1}$. Here, $\delta = 0.47$ and $\beta = 2/3$ are numerical constants originally used for columnar grains and obtained from Ref. 45. The effective "domain" size D_a in this model is expected to be equal to the average distance between the tracks. Based on the estimate for the fraction of the damaged volume obtained from direct impact model $\alpha = \alpha_0(1 - e^{-\sigma\Phi})$,^{46,47} we obtain

$$D_a^{-1} = D_0^{-1}(1 - e^{-\sigma\Phi}), \quad (3)$$

where α is a disorder parameter, D_0 is the maximum domain size, σ is a damaged cross section, and Φ is the ion fluence.

B. The lower limit for thermal conductivity of amorphous Al_2O_3

The lowest value of thermal conductivity is evaluated based on the expression by Cahill *et al* for minimal thermal conductivity,⁴⁸

$$k_{\min} = \left(\frac{\pi}{6}\right)^{\frac{1}{3}} k_B \Omega_0^{\frac{2}{3}} \sum_i v_i \left(\frac{T}{\Theta_i}\right) \int_0^{\frac{T}{\Theta_i}} \frac{x^3 e^x}{(e^x - 1)^2} dx, \quad (4)$$

where Θ_i is the Debye temperature and all other parameters were previously defined in Eq. (1). Equation (4) is valid for fully dense amorphous materials and highly disordered crystals.⁴⁹ This

expression has been also applied to materials with small voids.⁵⁰ The estimated minimal thermal conductivity is based on an amorphous sapphire density of 2.95 g/cm^3 , which was obtained from the literature,⁵¹ and results in $k_{\min} \sim 1.55 \text{ W/m K}$.

IV. RESULTS AND DISCUSSION

Transient TDTR signals measured for samples with different irradiation fluences at modulation frequency $f = 10 \text{ MHz}$ are shown in Fig. 2. The observed trend for decreasing ratio of in-phase (V_{in}) to out-of-phase (V_{out}) components of lock-in signal with an increase of irradiation fluence is similar to that reported for ion irradiated SiC samples and is attributed to the reduction of thermal conductivity.³⁰

The measurements were performed across a 1–10 MHz frequency range, and the results are shown in Fig. 3. The effective thermal conductivities k_{eff} shown in Fig. 3 were determined assuming a uniform thermal conductivity across the ion damaged layer. Evaluation of k_{eff} follows a standard procedure used in TDTR analysis for determining thermal conductivity of the substrate, which includes fitting of the substrate conductivity and thermal interface resistance with the metal transducer layer.³⁴ The error bars presented here reflect uncertainty in the transducer film thickness and sensitivity to fitted parameter. The latter was estimated using the Levenberg–Marquardt method.^{52,53} This involves numerical evaluation of the Jacobian matrix using $J_{ik} = \frac{\partial H}{\partial \gamma_k} = \frac{H(\gamma_k + \Delta \gamma_k, t_i) - H(\gamma_k, t_i)}{\Delta \gamma_k}$, where the subscript i enumerates data points measured at each delay time t_i , k enumerates the fitting parameters γ_k , and H is the calculated value of TDTR signal. All other parameters such as thermal properties of different materials are assumed to be accurately

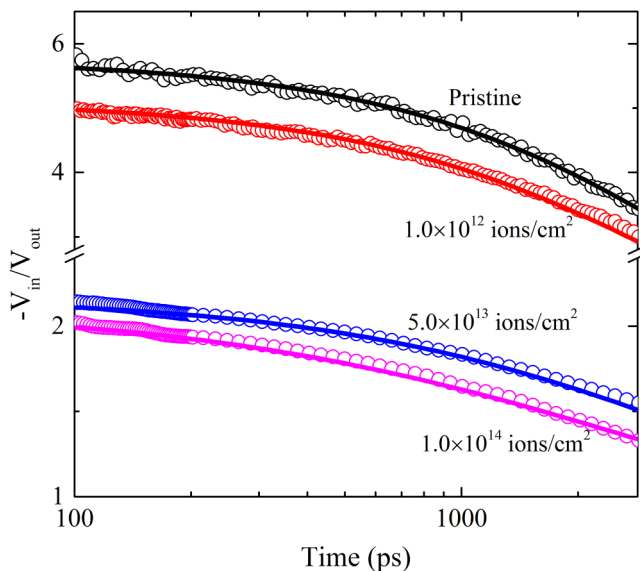


FIG. 2. Transient TDTR signal measured at $f = 10 \text{ MHz}$ for pristine and SHI irradiated sapphire samples at different fluences. Open circles represent experiment and solid lines represent fitting model.

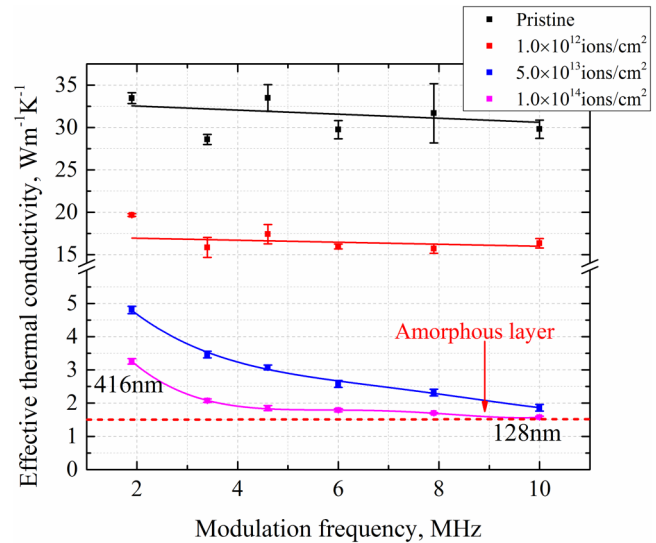


FIG. 3. Measured effective thermal conductivity k_{eff} of virgin and SHI irradiated sapphire as a function of pump beam modulation frequency neglecting the amorphous layer. The dots represent experimental data and solid lines serve as a guide to the eye to demonstrate frequency dependence of measured k_{eff} . Red dashed line shows the minimum thermal conductivity of amorphous sapphire based on Ref. 48.

known. This analysis clearly demonstrates a gradual reduction of k_{eff} with an increase of ion fluence, which is consistent with the previous work.^{13–15,17,27–29} A fairly constant k_{eff} is detected in pristine and SHI irradiated sapphire at small ion dose, i.e., for the fluence of $1.0 \times 10^{12} \text{ ions/cm}^2$ across all modulation frequencies. For two large dose samples, i.e., 5.0×10^{13} and $1.0 \times 10^{14} \text{ ions/cm}^2$, the measured values exhibit a notable dependence on the modulation frequency, where k_{eff} is lower at a higher modulation rate.

To understand this behavior, we need to consider the details of the microstructural changes induced by swift Xe ions. Nuclear and electronic energy loss profiles of 167 MeV Xe ions in Al_2O_3 calculated using SRIM 2013 code are shown in Fig. 4.⁵⁴ It is well documented that over the range where the electronic stopping power is above 10 keV/nm , the ion tracks are formed, whose density (TEM visible tracks) gradually increases with fluence and saturates at the dose of about $4.0 \times 10^{12} \text{ ions/cm}^2$.²⁴ This saturation is attributed to partial annealing of the ion tracks when they overlap and was confirmed by molecular dynamic simulations.^{24,55} Below the discontinuous ion track region extending down to $7.6 \mu\text{m}$,²² additional peak damage layer induced by nuclear stopping exists. For current samples, the calculated peak damage is located in the $9\text{--}12 \mu\text{m}$ range as shown in Fig. 4(a). However, a submicrometer depth probed by TDTR does not capture this peak damage region. Therefore, for $1.0 \times 10^{12} \text{ ions/cm}^2$ sample, the use of an effective single layer is justified and no frequency dependence of k_{eff} was observed, as evidenced from Fig. 3.

There is strong experimental evidence that at sufficiently high doses, the ion tracks undergo extensive overlapping where crystal structure experiences significant disordering, ultimately leading

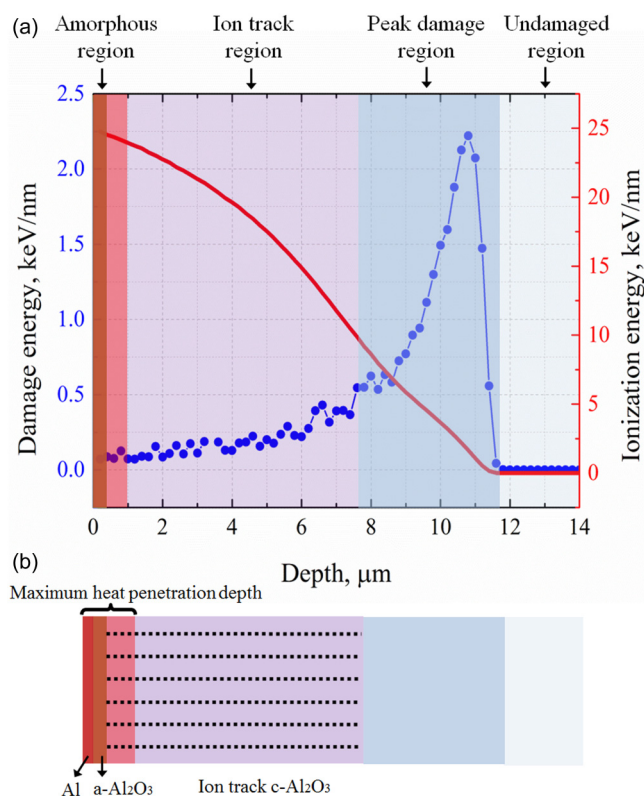


FIG. 4. (a) Cross-sectional damage profile in high dose irradiated sapphire calculated using SRIM 2013 code.⁵⁴ (b) Schematic representation of damage profile by three layers [Al (85 nm)/a-Al₂O₃/ion track c-Al₂O₃].

to formation of an amorphous layer. Previously reported thickness of the amorphous layer is 250 nm–500 nm^{56,57} at the fluence of 2.0×10^{14} ions/cm² and 800 nm at 3.5×10^{14} ions/cm².⁵⁸ The minimum threshold fluence for amorphization has been reported to be $\sim 2.0 \times 10^{13}$ ions/cm² for 90.3 MeV Xe ions⁵⁷ and $\sim 1.0 \times 10^{14}$ ions/cm² for 80 MeV Xe ions.⁵⁸

Therefore, at high fluences, the *nonuniform damage profile* probed by TDTR effectively represented by amorphized and ion track regions [Fig. 4(a)] is postulated to be responsible for the modulation frequency dependence of k_{eff} reported in Fig. 3. It is important to note that the k_{eff} degradation curve achieves saturation at fluences $>10^{13}$ ions/cm², when the amorphization begins.

Thermal conductivities of each individual layer in the aforementioned *nonuniform ion-affected region* can be determined if we consider a multilayer thermal model.^{52,59} Before discussing the details of a *multilayer data analysis*, we present some initial conclusions that simplify further analysis without diminishing physical insight. We start by considering the penetration depth of the thermal waves typically estimated using $D_{th} = \sqrt{k_{eff}/\pi Cf}$, where f is the modulation frequency and C is the volumetric heat capacity. For a sample irradiated with a fluence of 10^{12} ions/cm², whose conductivity was determined to be around 16 W/m K, the diffusion

length at 1.9–10 MHz is estimated to be between 0.90 and 0.39 μm , which implies that only a damage region characterized by ion tracks is probed. This combined with the absence of *amorphous layer* is the reason for negligible frequency dependence in k_{eff} as shown in Fig. 3.

For the largest dose sample, $k_{eff} = 1.6$ W/m K measured at 10 MHz is comparable to the lowest conductivity of Al₂O₃ evaluated using Eq. (4). Additionally, using measured k_{eff} values, the penetration depth of $D_{th} = 128$ and 416 nm at $f = 10$ and 1.9 MHz, respectively, is estimated. This suggests that the *largest dose sample underwent amorphization* with a thickness of the affected (amorphized) zone on the order of 100 nm. This observation is in agreement with our HRTEM results (discussed below) and earlier measurements of amorphization in SHI irradiated sapphire.^{23,56,58}

Using this qualitative analysis, we attribute the frequency dependence of k_{eff} in high dose samples to a weighted *average of amorphous and ion track layer conductivities*, where lower modulation frequency, i.e., equivalently longer penetration, response has a larger contribution from the ion track region whose conductivity is expected to be larger than that of the amorphous layer. We conclude that the multilayer analysis of the two largest dose samples should include both the amorphous and ion track regions, while the peak damage region can be neglected as the thermal waves do not penetrate deeper than 1 μm below samples surface for the modulation frequencies used in this work.

Our comprehensive analysis of TDTR signals from amorphized samples is based on the multilayer representation of the damage region.^{52,59} Specifically, we implement thermal data analysis based on *three layers* (Al/a-Al₂O₃/ion track Al₂O₃) as depicted in Fig. 4(b) for two high dose samples (5.0×10^{13} and 1.0×10^{14} ions/cm²) to extract thermal conductivity of the damaged layer. In the case of the highest dose sample (1.0×10^{14} ions/cm²), it was possible to measure the thickness of the amorphous layer using XTEM analysis as shown in Fig. 5 with corresponding selected area diffraction (SAD) patterns. From this electron microscopy analysis, the presence of the amorphous layer was confirmed and its thickness was measured to be ~ 189 nm. Corresponding energy dispersive spectroscopy (EDS) scan of the amorphous Al₂O₃ layer shows a slightly higher concentration of oxygen in the first few nanometers after which a relatively stable 40% Al and 60% oxygen (O) is achieved. We analyzed the highest dose sample (1.0×10^{14} ions/cm²) using multifrequency analysis taking amorphous layer thickness obtained from TEM to determine thermal conductivities of the ion track region and amorphous layers as 4.6 ± 0.1 and 1.9 ± 0.1 W/m K, respectively. In the analysis of 5.0×10^{13} ions/cm² sample, the conductivity of the amorphous layer determined in the previous case was assumed to be known, and thermal conductivity of the ion track region layer and the thickness of amorphous layer were used as fitting parameters. This multifrequency analysis was performed on all four samples, and the results are listed in Table I.

The conductivity values presented in Table I for pristine and low dose sample (1.0×10^{12} ions/cm²) are close to that of the measured from single frequency analysis. This reaffirms our earlier conclusion that frequency dependence of k_{eff} is because of the presence of an extra amorphous layer at the top. As seen from the table, our measured a-Al₂O₃ thickness is in the range of previously reported

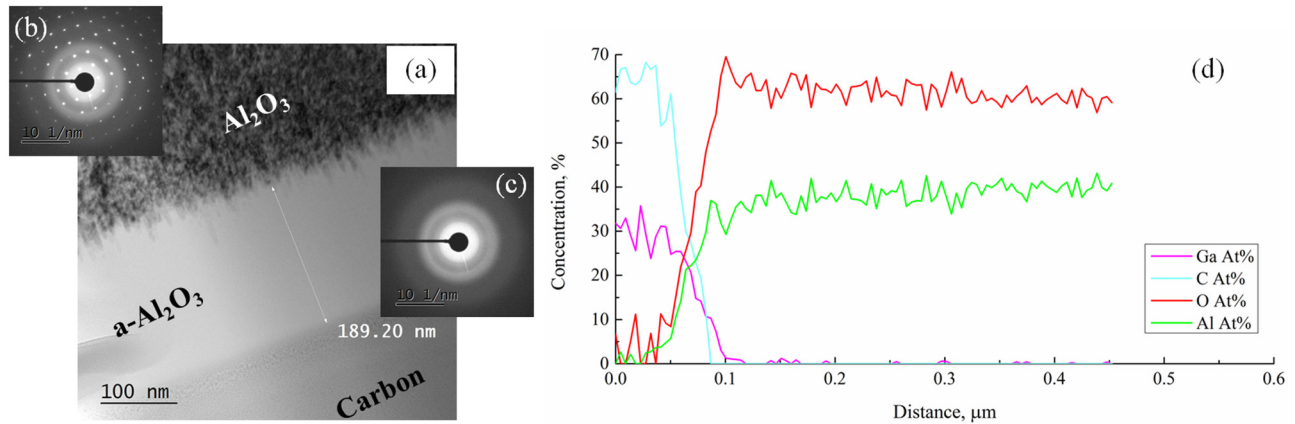


FIG. 5. (a) Bright field XTEM of sapphire irradiated with 1.0×10^{14} ions/cm² 167 MeV Xe ions. (b) and (c) are SAD patterns from the subsurface region indicating crystalline structure and amorphous layers, respectively. (d) EDS line scan starting from the protective carbon layer on the left of the image, through the amorphous Al₂O₃ zone, and ending in the crystalline Al₂O₃ on the right. Ga is present in the protective carbon layer from the FIB used to deposit it. Carbon was deposited on the Al₂O₃ surface prior to trench milling during FIB lamella preparation in order to protect the surface from FIB induced damage.

values of 50 and 120 nm, determined by Rutherford backscattering spectrometry in channelling geometry (RBS-C)⁵⁷ where the same Xe ions were used, but with a lower Xe ion energy of 90.3 MeV. In Ref. 56, the amorphous layer of ~500 nm was measured using TEM at a fluence of 2.0×10^{14} ion/cm² with a Xe ion energy of 92 MeV.

We employed the phonon-mediated thermal transport model defined by Eqs. (1)–(3) to analyze reduction of thermal conductivity in the irradiated samples. First, we determined the value of $A_0 = 1.0 \times 10^{-46}$ s³ by fitting intrinsic thermal conductivity of the pristine sapphire sample. Next, we analyzed irradiated samples. This did not consider anisotropic effects that may arise from the aligned structure of the ion tracks parallel to the c-axis. Also, the impact of nondiffusive behavior of phonons with mean free paths longer than thermal diffusion length was not considered.³⁷ Systematic analysis of these effects falls beyond the scope of this work but is expected to be a contributing factor in the future analysis.

The experimental thermal conductivity data were fitted using Eq. (1) and are shown as a solid line in Fig. 6. The solid line corresponds to the best fit of experimental data with the model using the average distance between ion tracks $D_0 = 14$ nm and damage cross section $\sigma = 2.0 \times 10^{-13}$ cm² as fitting parameters. The model captures the gradual decrease of thermal conductivity until it levels off due to saturation of ion track density reported in previous studies.^{23,24} Horizontal line corresponds to k_{min} calculated using

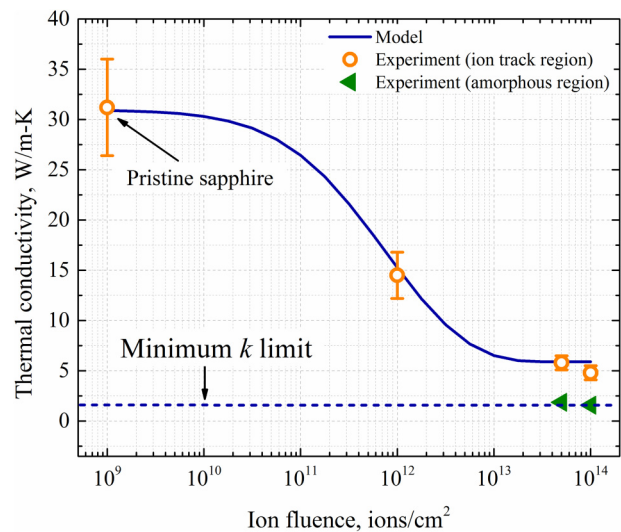


FIG. 6. Measured values (green triangles—amorphous layer and orange circles—ion track region) and fitted thermal conductivity (blue line) of sapphire vs ion fluence in the SHI regime. Blue dashed line represents k_{min} for amorphous sapphire obtained from Eq. (4).

TABLE I. Fitting results from heat diffusion models based on three layer (Al/a-Al₂O₃/Al₂O₃) representation of damage profile. G is the interface resistance, k is the thermal conductivity, and d is the thickness.

| Fluence (ions/cm ²) | G of a-Al ₂ O ₃ –Al (m ² K/W) measured by TDTR | $k_{ion\ track\ layer}$ (W/m K) measured by TDTR | $k_{amorph\ layer}$ (W/m K) measured by TDTR | $d_{amorph\ layer}$ (nm) measured by TDTR |
|---------------------------------|---|--|--|---|
| Pristine | $(1.8 \pm 0.2) \times 10^{-8}$ | 31.2 ± 4.8 | ... | ... |
| 1.0×10^{12} | $(1.5 \pm 0.1) \times 10^{-8}$ | 14.5 ± 2.3 | ... | ... |
| 5.0×10^{13} | $(1.2 \pm 0.4) \times 10^{-8}$ | 5.8 ± 0.7 | ... | 122.8 ± 18.3 |
| 1.0×10^{14} | $(2.1 \pm 1.7) \times 10^{-8}$ | 4.8 ± 0.7 | 1.9 ± 0.1 | ... |

Eq. (4) is in agreement with experimental results. The fitted values for D_0 and σ are larger than 3.4 nm and $1.2 \times 10^{-13} \text{ cm}^2$ reported in the literature because of the effective domain size approximation. This can also be attributed to the fact that present simplified analysis considers only the analytical form of the anharmonic scattering term [Eq. (4)], which results in inaccurate representation of the spectral contribution of phonons with different phonon mean free path (mfp).⁶⁰ This simple expression for anharmonic phonon scattering rate tends to shift the weight distribution toward a lower mfp phonons. More accurate representation of the anharmonic term remains a subject of a future work.

V. CONCLUSION

We have performed cross-plane thermal conductivity measurements of pristine and SHI irradiated sapphire samples at various ion doses. We demonstrated the use of modulation frequency-dependent TDTR to probe the conductivity variation in nanometer-scale thick ion irradiated subsurface regions. TDTR measurement revealed that the amorphous phase is formed only in the case of high dose irradiation and it was shown that thickness of this amorphous layer can be accurately measured using this technique. This demonstration opens up opportunities for further research on nano-to-micrometer thermal depth profiling in ion beam modified insulators to isolate the impact of damage resulting from inelastic electronic stopping (on a nanometer scale) and from elastic nuclear stopping (on a micrometer scale) on subsurface thermal conduction.

ACKNOWLEDGMENTS

A.A. and Z.N.U. acknowledge funding support by Kazakhstan Ministry of Education and Science under Grant No. AP05130446 and State-Targeted Program No. BR05236454, by Kazakhstan Ministry of Industry and Infrastructural Development under Grant No. AP06851392, and by Nazarbayev University under FDCR Grant No. 110119FD4501. V.S.C. and M.K. acknowledge support by the Centre for Thermal Energy Transport under Irradiation (TETI) an Energy Frontier Research Centre funded by the U.S. Department of Energy, Office of Science, and Office of Basic Energy Sciences.

REFERENCES

- ¹M. Nastasi and J. W. Mayer, *Ion Implantation and Synthesis of Materials* (Springer, Berlin, 2006), Vol. 80.
- ²W. Wesch, E. Wendler, and G. Götz, "Defect production during ion implantation of various $A_{III}B_V$ semiconductors," *J. Appl. Phys.* **65**, 519–526 (1989).
- ³L. Ma, Y. Tan, M. Ghorbani-Asl, R. Boettger, S. Kretschmer, S. Zhou, Z. Huang, A. V. Krashennnikov, and F. Chen, "Tailoring the optical properties of atomically-thin WS₂ via ion irradiation," *Nanoscale* **9**(31), 11027–11034 (2017).
- ⁴C. Gómez-Navarro, P. J. De Pablo, J. Gómez-Herrero, B. Biel, F. J. García-Vidal, A. Rubio, and F. Flores, "Tuning the conductance of single-walled carbon nanotubes by ion irradiation in the Anderson localization regime," *Nat. Mater.* **4**(7), 534–539 (2005).
- ⁵W. J. Weber, D. M. Duffy, L. Thomé, and Y. Zhang, "The role of electronic energy loss in Ion beam modification of materials," *Curr. Opin. Solid State Mater. Sci.* **19**, 1 (2015).
- ⁶J. Olivares, M. L. Crespillo, O. Caballero-Calero, M. D. Ynsa, A. García-Cabañes, M. Toulemonde, C. Trautmann, and F. Agulló-López, "Thick

optical waveguides in lithium niobate induced by swift heavy ions ($\sim 10 \text{ MeV}$ amu) at ultralow fluences," *Opt. Express* **17**, 24175–24182 (2009).

- ⁷A. Hadley, C. Notthoff, P. Mota-Santiago, U. H. Hossain, N. Kirby, M. E. Toimil-Molares, and P. Kluth, "Etched ion tracks in amorphous SiO₂ characterized by small angle x-ray scattering: Influence of ion energy and etching conditions," *Nanotechnology* **30**, 274001 (2019).
- ⁸Z. Tian, S. Lee, and G. Chen, "Comprehensive review of heat transfer in thermoelectric materials and devices," *Annu. Rev. Heat Transfer* **17**, 425–483 (2014).
- ⁹D. G. Cahill, P. V. Braun, G. Chen, D. R. Clarke, S. Fan, K. E. Goodson, P. Keblinski, W. P. King, G. D. Mahan, A. Majumdar, H. J. Maris, S. R. Phillpot, E. Pop, and L. Shi, "Nanoscale thermal transport. II. 2003–2012," *Appl. Phys. Rev.* **1**, 011305 (2014).
- ¹⁰D. R. Clarke and S. R. Phillpot, "Thermal barrier coating materials," *Mater. Today* **8**, 22–29 (2005).
- ¹¹B. J. Marsden, M. Haverty, W. Bodel, G. N. Hall, A. N. Jones, P. M. Mummery, and M. Treifi, "Dimensional change, irradiation creep and thermal/mechanical property changes in nuclear graphite," *Int. Mater. Rev.* **61**, 155–182 (2016).
- ¹²B. Deng, A. Chernatynskiy, P. Shukla, S. B. Sinnott, and S. R. Phillpot, "Effects of edge dislocations on thermal transport in UO₂," *J. Nucl. Mater.* **434**, 203–209 (2013).
- ¹³M. Khafizov, J. Pakarinen, L. He, and D. H. Hurley, "Impact of irradiation induced dislocation loops on thermal conductivity in ceramics," *J. Am. Ceram. Soc.* **102**, 7533–7542 (2019).
- ¹⁴F. Hofmann, D. R. Mason, J. K. Eliason, A. A. Maznev, K. A. Nelson, and S. L. Dudarev, "Non-contact measurement of thermal diffusivity in ion-implanted nuclear materials," *Sci. Rep.* **5**, 16042 (2015).
- ¹⁵M. Khafizov, V. Chauhan, Y. Wang, F. Riyad, N. Hang, and D. Hurley, "Investigation of thermal transport in composites and ion beam irradiated materials for nuclear energy applications," *J. Mater. Res.* **32**, 204–216 (2017).
- ¹⁶C. A. Dennett, K. P. So, A. Kushima, D. L. Buller, K. Hattar, and M. P. Short, "Detecting self-ion irradiation-induced void swelling in pure copper using transient grating spectroscopy," *Acta Mater.* **145**, 496–503 (2018).
- ¹⁷L. David, S. Gomès, G. Garlot, J.-P. Roger, D. Fournier, C. Valot, and M. Raynaud, "Characterization of thermal conductivity degradation induced by heavy ion irradiation in ceramic materials," *J. Phys. D Appl. Phys.* **41**, 035502 (2008).
- ¹⁸R. I. Palomares, C. L. Tracy, F. Zhang, C. Park, D. Popov, C. Trautmann, R. C. Ewing, and M. Lang, "In situ defect annealing of swift heavy ion irradiated CeO₂ and ThO₂ using synchrotron X-ray diffraction and a hydrothermal diamond anvil cell," *J. Appl. Crystallogr.* **48**, 711–717 (2015).
- ¹⁹C. Ronchi, M. Sheidlin, D. Staicu, and M. Kinoshit, "Effect of burn-up on the thermal conductivity of uranium dioxide up to 100.000 MWd⁻¹," *J. Nucl. Mater.* **327**, 58 (2004).
- ²⁰P. Kluth, O. H. Pakarinen, F. Djurabekova, R. Giuliani, M. C. Ridgway, A. P. Byrne, and K. Nordlund, "Nanoscale density fluctuations in swift heavy ion irradiated amorphous SiO₂," *J. Appl. Phys.* **110**, 123520 (2011).
- ²¹L. Thomé, A. Debelle, F. Garrido, S. Mylonas, B. Décamps, C. Bachelet, G. Sattonnay, S. Moll, S. Pellegrino, S. Miro, and P. Trocellier, "Radiation effects in nuclear materials: Role of nuclear and electronic energy losses and their synergy," *Nucl. Instrum. Methods Phys. Res. B* **307**, 43–48 (2013).
- ²²V. A. Skuratov, J. O'Connell, N. S. Kirilkin, and J. Neethling, "On the threshold of damage formation in aluminium oxide via electronic excitations," *Nucl. Instrum. Methods Phys. Res. B* **326**, 223–227 (2014).
- ²³A. Kabir, A. Meftah, J. P. Stoquert, M. Tolemonde, I. Monnet, and M. Izerrouken, "Structural disorder in sapphire induced by 90.3 MeV xenon ions," *Nucl. Instrum. Methods Phys. Res. B* **268**, 3195–3198 (2010).
- ²⁴J. H. O'Connell, R. A. Rymzhanov, V. A. Skuratov, A. E. Volkov, and N. S. Kirilkin, "Latent tracks and associated strain in Al₂O₃ irradiated with swift heavy ions," *Nucl. Instrum. Methods Phys. Res. B* **374**, 97–101 (2016).
- ²⁵N. Itoh, D. M. Duffy, S. Khakshouri, and A. M. Stoneham, "Making tracks: Electronic excitation roles in forming swift heavy ions," *J. Phys. Condens. Matter* **21**, 474205 (2009).

- ²⁶L. L. Snead, S. J. Zinkle, and D. P. White, "Thermal conductivity degradation of ceramic materials due to low temperature, low dose neutron irradiation," *J. Nucl. Mater.* **340**, 187–202 (2005).
- ²⁷C. Jensen, M. Chirtoc, N. Horny, J. S. Antoniow, H. Pron, and H. Ban, "Thermal conductivity profile determination in proton-irradiated ZrC by spatial and frequency scanning thermal wave methods," *J. Appl. Phys.* **114**, 133509 (2013).
- ²⁸P. B. Weissensee, J. P. Feser, and D. G. Cahill, "Effect of ion irradiation on the thermal conductivity of UO_2 and U_3O_8 epitaxial layers," *J. Nucl. Mater.* **443**, 212–217 (2013).
- ²⁹R. Cheaito, C. S. Gorham, A. Misra, K. Hattar, and P. E. Hopkins, "Thermal conductivity measurements via time-domain thermoreflectance for the characterization of radiation induced damage," *J. Mater. Res.* **30**, 1403–1412 (2015).
- ³⁰V. S. Chauhan, M. F. Riyad, X. Du, C. Wei, B. Tyburska-Püschel, J. C. Zhao, and M. Khafizov, "Thermal conductivity degradation and microstructural damage characterization in low-dose ion beam-irradiated 3C-SiC," *Mater. Mater. Trans. E* **4**, 61–69 (2017).
- ³¹Y. Zhao, D. Liu, J. Chen, L. Zhu, A. Belianinov, O. S. Ovchinnikova, R. R. Unocic, M. J. Burch, S. Kim, H. Hao, D. S. Pickard, B. Li, and J. T. L. Thong, "Engineering the thermal conductivity along an individual silicon nanowire by selective helium ion irradiation," *Nat. Commun.* **8**, 15919 (2017).
- ³²J. Zhu, D. Tang, W. Wang, J. Liu, K. W. Holub, and R. Yang, "Ultrafast thermoreflectance techniques for measuring thermal conductivity and interface thermal conductance of thin films," *J. Appl. Phys.* **108**, 094315 (2010).
- ³³J. Liu, J. Zhu, M. Tian, X. Gu, A. Schmidt, and R. Yang, "Simultaneous measurement of thermal conductivity and heat capacity of bulk and thin film materials using frequency-dependent transient thermoreflectance method," *Rev. Sci. Instrum.* **84**, 034902 (2013).
- ³⁴D. G. Cahill, "Analysis of heat flow in layered structures for time-domain thermoreflectance," *Rev. Sci. Instrum.* **75**, 5119 (2004).
- ³⁵V. A. Skuratov, D. L. Zagorski, A. E. Efimov, V. A. Kluev, Y. P. Toporov, and B. V. Mchedlishvili, "Swift heavy ion irradiation effect on the surface of sapphire single crystals," *Radiat. Meas.* **34**, 571–576 (2001).
- ³⁶V. A. Skuratov, S. J. Zinkle, A. E. Efimov, and K. Havancsak, "Swift heavy ion-induced modification of Al_2O_3 and MgO surfaces," *Nucl. Instrum. Methods Phys. Res. B* **203**, 136–140 (2003).
- ³⁷Y. K. Koh and D. G. Cahill, "Frequency dependence of the thermal conductivity of semiconductor alloys," *Phys. Rev. B* **76**, 075207 (2007).
- ³⁸V. S. Chauhan, A. Abdullaev, Z. Utegulov, J. O'Connell, V. Skuratov, and M. Khafizov, "Simultaneous characterization of cross- and in-plane thermal transport in insulator patterned by directionally aligned nano-channels," *AIP Adv.* **10**, 015304 (2020).
- ³⁹P. G. Klemens, "Thermal conductivity and lattice vibrational modes," *Solid State Phys.* **7**, 1–98 (1958).
- ⁴⁰M. Khafizov, I.-W. Park, A. Chernatynskiy, L. He, J. Lin, J. J. Moore, D. Swank, T. Lillo, S. R. Phillpot, A. El-Azab, and D. H. Hurley, "Thermal conductivity in nanocrystalline ceria thin films," *J. Am. Ceram. Soc.* **97**, 562–569 (2013).
- ⁴¹H. Bialas, O. Weis, and H. Wendel, "Dispersion of acoustic phonons in sapphire," *Phys. Lett. A* **43**, 97–98 (1973).
- ⁴²G. A. Slack, "Thermal conductivity of MgO , Al_2O_3 , MgAl_2O_4 and Fe_3O_4 crystals from 3 to 300 K," *Phys. Rev. Lett.* **126**, 427 (1962).
- ⁴³T. Goto, O. L. Anderson, I. Ohno, and S. Yamamoto, "Elastic constants of corundum up to 1825K," *J. Geophys. Res.* **94**, 7588–7602 (1989).
- ⁴⁴A. J. H. McGaughey, E. S. Landry, D. P. Sellan, and C. H. Amon, "Size-dependent model for thin film and nanowire thermal conductivity," *Appl. Phys. Lett.* **99**, 131904 (2011).
- ⁴⁵Z. Wang, J. E. Alaniz, W. Jang, J. E. Garay, and C. Dames, "Thermal conductivity of nanocrystalline silicon: Importance of grain size and frequency-dependent mean free paths," *Nano Lett.* **11**, 2206–2213 (2011).
- ⁴⁶B. Canut, A. Benyagoub, G. Marest, A. Meftah, N. Moncoffre, S. M. M. Ramos, F. Studer, P. Thevenard, and M. Toulemonde, "Swift-uranium-ion-induced damage in sapphire," *Phys. Rev. B* **51**, 12194 (1995).
- ⁴⁷W. J. Weber, "Models and mechanisms of irradiation-induced amorphization in ceramics," *Nucl. Instrum. Methods Phys. Res. B* **166–167**, 98–106 (2000).
- ⁴⁸D. G. Cahill, S. K. Watson, and R. O. Pohl, "Lower limit to the thermal conductivity of disordered crystals," *Phys. Rev. B* **46**, 6131 (1992).
- ⁴⁹M. C. Wingert, J. Zheng, S. Kwon, and R. Chen, "Thermal transport in amorphous materials: A review," *Semicond. Sci. Technol.* **31**, 113003 (2016).
- ⁵⁰R. M. Costescu, A. J. Bullen, G. Matamis, K. E. O'Hara, and D. G. Cahill, "Thermal conductivity and sound velocities of hydrogen-silsesquioxane low-k dielectrics," *Phys. Rev. B* **65**, 094205 (2002).
- ⁵¹A. Cappella, J.-L. Battaglia, V. Schick, A. Kusiak, A. Lamperti, C. Wiemer, and B. Hay, "High temperature thermal conductivity of amorphous Al_2O_3 thin films grown by low temperature ALD," *Adv. Eng. Mater.* **15**, 1046–1050 (2013).
- ⁵²M. F. Riyad, V. Chauhan, and M. Khafizov, "Implementation of a multilayer model for measurement of thermal conductivity in ion beam irradiated samples using a modulated thermoreflectance approach," *J. Nucl. Mater.* **509**, 134–144 (2018).
- ⁵³H. P. Gavin, "The Levenberg-Marquardt method for nonlinear least squares curve-fitting problems" Duke University (2013).
- ⁵⁴J. F. Ziegler, M. D. Ziegler, and J. P. Biersack, "SRIM—The Stopping and range of ions in matter," *Nucl. Instrum. Methods Phys. Res. B* **268**, 1818–1823 (2010).
- ⁵⁵R. A. Rymzhanov, N. Medvedev, A. E. Volkov, J. H. O'Connell, and V. A. Skuratov, "Overlap of swift heavy ion tracks in Al_2O_3 ," *Nucl. Instrum. Methods Phys. Res. B* **435**, 121–125 (2018).
- ⁵⁶C. Grygiel, F. Moisy, M. Sall, H. Lebius, E. Balanzat, T. Madi, T. Been, D. Marie, and I. Monnet, "In-situ kinetics of modifications induced by swift heavy ions in Al_2O_3 : Colour centre formation, structural modification and amorphization," *Acta Mater.* **140**, 157–167 (2017).
- ⁵⁷A. Kabir, A. Meftah, J. P. Stoquert, M. Toulemonde, and I. Monnet, "Amorphization of sapphire induced by swift-heavy ions: A two-step process," *Nucl. Instrum. Methods Phys. Res. B* **266**, 2976–2980 (2008).
- ⁵⁸N. Okubo, N. Ishikawa, M. Sataka, and S. Jitsukawa, "Surface amorphization in Al_2O_3 induced by swift heavy ion irradiation," *Nucl. Instrum. Methods Phys. Res. B* **314**, 208–210 (2013).
- ⁵⁹Z. Hua, A. Fleming, and H. Ban, "The study of using a multi-layered model to extract thermal property profiles of ion-irradiated materials," *Int. J. Heat Mass Transf.* **131**, 206–216 (2019).
- ⁶⁰K. M. Hoogeboom-Pot, J. N. Hernandez-Charpak, X. Gu, T. D. Frazer, E. H. Anderson, W. Chao, R. W. Falcone, R. Yang, M. Murnane, H. C. Kapteyn, and D. Nardi, "A new regime of nanoscale thermal transport: Collective diffusion increases dissipation efficiency," *Proc. Natl. Acad. Sci. U.S.A.* **112**, 4846–4851 (2015).